



## Generation of Retinal Pigment Epithelial Cells from Small Molecules and *OCT4* Reprogrammed Human Induced Pluripotent Stem Cells

TIM U. KROHNE,<sup>a\*</sup> PETER D. WESTENSKOW,<sup>a\*</sup> TOSHIHIDE KURIHARA,<sup>a</sup> DAVID F. FRIEDLANDER,<sup>a</sup> MANDY LEHMANN,<sup>a</sup> ALISON L. DORSEY,<sup>a</sup> WENLIN LI,<sup>b</sup> SAIYONG ZHU,<sup>b</sup> ANDREW SCHULTZ,<sup>c</sup> JUNHUA WANG,<sup>c</sup> GARY SIUZDAK,<sup>b,c</sup> SHENG DING,<sup>b</sup> MARTIN FRIEDLANDER<sup>a</sup>

**Key Words.** Retina • Induced pluripotent stem cells • Differentiation • Small molecules • Stem cell transplantation • Aging

### ABSTRACT

**Autologous retinal pigment epithelium (RPE) grafts derived from induced pluripotent stem cells (iPSCs) may be used to cure blinding diseases in which RPE dysfunction results in photoreceptor degeneration. Four-, two-, and one-factor-derived iPSCs (4F-, 2F-, and 1F-iPSCs, respectively) were differentiated into fully functional cuboidal pigmented cells in polarized monolayers that express RPE-specific markers. 1F-iPSC-RPE (1F-iPS-RPE) strongly resembles primary human fetal RPE (hFRPE) based on proteomic and untargeted metabolomic analyses, and using novel in vivo imaging technology coupled with electroretinography, we demonstrated that 1F-iPS-RPE mediate anatomical and functional rescue of photoreceptors after transplantation in an animal model of RPE-mediated retinal degeneration. 1F-iPS-RPE cells were injected subretinally as a suspension and formed a monolayer dispersed between host RPE cells. Furthermore, 1F-iPS-RPE do not simply provide trophic support to rescue photoreceptors as previously speculated but actually phagocytose photoreceptor outer segments in vivo and maintain visual cycling. Thus, 1F-iPS-RPE grafts may be superior to conventional iPS-RPE for clinical use because 1F-iPS-RPE closely resemble hFRPE, mediate anatomical and functional photoreceptor rescue in vivo, and are generated using a reduced number of potentially oncogenic reprogramming factors. STEM CELLS TRANSLATIONAL MEDICINE 2012;1:96–109**

### INTRODUCTION

One of the most significant recent breakthroughs in stem cell research was adult somatic cell reprogramming into pluripotent stem cells [1, 2] that can be differentiated into autologous grafts for therapeutic reimplantation in various diseases [3]. The use of induced pluripotent stem cells (iPSCs) circumvents most of the ethical and practical problems associated with large-scale clinical use of embryonic stem cells (ESCs), and patients with induced pluripotent stem cell (iPSC)-derived autologous transplants may not require life-long immunosuppressive treatments to prevent graft rejection. However, safety concerns regarding iPSCs include malignant transformation resulting from reactivation of the four reprogramming transcription factors (including *c-MYC*) randomly integrated into the genome at multiple loci following retroviral transduction. In fact, iPSC generation and transformation share many molecular mechanisms, and a high incidence of tumorigenesis is observed in

iPSC-derived chimeric mice [4–7]. The risk of tumorigenesis cannot be attributed solely to *c-MYC* reactivation; transgenic mice derived from iPSCs without *c-MYC* still form tumors [8].

Exhaustive comparative analyses of multiple human iPSC (hiPSC) and human embryonic stem cell (hESC) lines reveal that although many hiPSC and hESC lines share very similar transcriptomic and epigenetic profiles, others are heterogeneous. The differences observed are randomly distributed and limit the differentiation capacity of the cells [9]. Furthermore, recent evidence shows that in hiPSCs, reprogramming and selection pressure to obtain rapidly proliferating cell lines may induce chromosomal aneuploidy in nonrandomly distributed loci that may further limit the differentiation capacity and promote tumorigenicity of iPSCs [10–12]. Genetic instability in iPSCs is correlated with higher passage numbers, so reprogramming methods that are inefficient and require multiple passages may increase the risk of tumorigenesis [10, 11]. Furthermore, high cytotoxicity is observed when reprogramming methods use repeated transfections

<sup>a</sup>Department of Cell Biology,<sup>b</sup>Department of Chemistry, and <sup>c</sup>Center for Metabolomics, The Scripps Research Institute, La Jolla, California, USA

\*Contributed equally as first authors.

Correspondence: Martin Friedlander, M.D., Ph.D., The Scripps Research Institute, MB 28, 10550 North Torrey Pines Road, La Jolla, California 92037, USA. Telephone: (858) 784-9138; Fax: (858) 784-2504; e-mail: friedlan@scripps.edu

Received November 22, 2011; accepted for publication January 4, 2012; first published online in SCTM EXPRESS February 6, 2012.

©AlphaMed Press  
1066-5099/2012/\$30.00/0

<http://dx.doi.org/10.5966/sctm.2011-0057>

(reprogramming methods involving mRNA strands or recombinant proteins). Consequently, these methods could induce even higher selection pressures for highly proliferative cells with mutations; however, this idea has not yet been directly tested.

To generate retinal pigment epithelium (RPE) cells from hiPSCs for treating diseases such as age-related macular degeneration (AMD) in which the onset occurs in humans aged 55 years and older, the source material (likely fibroblasts or keratinocytes) will be older and more difficult to reprogram. The RPE derivation process is long, and all clones will need to be carefully screened before transplantation. Consequently, this treatment strategy could be very economically taxing to patients and health care systems. Therefore, to generate any tissue of interest, including RPE cells, from hiPSCs, one or two specific reprogramming protocols may need to be adopted and optimized to ensure reliable and safe derivations of that cell type. Furthermore, experimental animals with implants should be monitored over extended periods of time to ensure that no tumors form. We have recently reported the generation of iPSCs reprogrammed using two or one factors (*OCT4/KLF4* or *OCT4* only) and small molecules [13, 14]. In this study, we examined the capacity of these one- or two-factor iPSCs to differentiate into RPE and provide novel evidence that they can be efficiently directed to RPE fates.

The RPE is a monolayer of pigmented cuboidal epithelial cells located at the interface between retinal photoreceptor cells and the underlying choriocapillaris that performs functions vital for photoreceptor survival [15]. RPE cell loss or dysfunction is the primary cause of many noncurable blinding diseases, such as AMD [15], the most common cause of legal blindness in developed countries [16, 17]. Experimental surgical approaches have demonstrated the feasibility and effectiveness of autologous RPE cell replacement therapy in AMD patients; however, these approaches are highly invasive and impractical [18, 19]. RPE cells derived from ESCs has been shown to provide temporary rescue in an animal model of RPE-mediated retinal degeneration, the Royal College of Surgeons (RCS) rat [20, 21]. However, it remains to be determined whether ESC-RPE cells can be safely implanted in long-term studies without host rejection. Alternatively, iPSCs may be generated from patient-derived epidermal cells and provide a readily accessible source of autologous RPE cell grafts. Human iPSCs can be converted into RPE cells [22–26] and provide temporary rescue effects after transplantation in rats [23]. However, the results of a comprehensive transcriptomic analysis of human ESC-RPE, conventional human iPS-RPE, and human fetal RPE (hFRPE) revealed that human iPS-RPE have a disparate transcriptomic profile from hFRPE [27], perhaps because of multiple integration events in the genome induced by the lentiviral delivery strategy [1, 28]. In contrast to previous studies, we used iPSCs reprogrammed by a novel approach that requires only one or two exogenous transcription factors. The elimination of oncogenic reprogramming factors may reduce the risk of tumor formation and enable derivation of human iPS-RPE that more closely resemble hFRPE. This could make these cells superior for clinical application.

## MATERIALS AND METHODS

### Generation and Maintenance of iPSCs

Generation and characterization of two-factor and one-factor iPSCs from neonatal keratinocytes (Lonza, Walkersville, MD, <http://www.lonza.com>) was described previously [13, 14] (Table

1). Four-factor (4F)-iPSCs were generated from human fetal lung fibroblasts (IMR-90; American Type Culture Collection, Manassas, VA, <http://www.atcc.org>) [1]. Cells were maintained in Dulbecco's modified Eagle's medium (DMEM)/Ham's F-12 medium (F12), supplemented with 2 mM glutamine, 0.1 mM nonessential amino acids, 0.1 mM  $\beta$ -mercaptoethanol, 100 U/ml penicillin, 100  $\mu$ g/ml streptomycin, 10 ng/ml basic fibroblast growth factor, and 20% Knockout serum replacement (all the components of the media were purchased from Invitrogen, Carlsbad, CA, <http://www.invitrogen.com>).

### Cell Culture and Differentiation Treatment

iPSCs were expanded to confluence in maintenance medium (12–14 days) before starting differentiation treatments. For spontaneous differentiation, differentiation medium consisting of Knockout DMEM, 2 mM glutamine, 0.1 mM nonessential amino acids, 0.1 mM  $\beta$ -mercaptoethanol, 100 U/ml penicillin, 100  $\mu$ g/ml streptomycin, and 20% Knockout serum replacement (Invitrogen) was added. For directed differentiation, 10 mM nicotinamide (Sigma-Aldrich, St. Louis, <http://www.sigmaaldrich.com>)/62 ng/ml activin A (Peprotech, Rocky Hill, NJ, <http://www.peprotech.com>) treatment was applied according to previously described protocols [20]. Ten weeks later, pigmented clustered were manually excised and replated on Matrigel (Becton, Dickinson and Company, Franklin Lakes, NJ, <http://www.bd.com>; 1:30)-coated plates. Cells were detached with 0.05% trypsin EDTA (Invitrogen) for subsequent expansion.

Naïve Hues9 (WiCell Research Institute, Madison, WI, <http://www.wicell.org>), 4F-, 2F-, and 1F-iPSCs were maintained in mouse embryonic fibroblast-conditioned medium until appropriate cell numbers were achieved. Neonatal keratinocytes and fetal fibroblasts were cultured according to the supplier's recommendations. To make primary human RPE (hRPE) cultures, anterior segments and neural retinas were removed from donor eyes (San Diego Eye Bank, San Diego, <http://www.sdeb.org>). The eye-cups were filled with trypsin EDTA and incubated for 30–45 minutes at 37°C before removing the RPE cells with blunt forceps. They were maintained in DMEM/F12 (Invitrogen) + 2%–10% fetal bovine serum (FBS) (Jackson ImmunoResearch Laboratories, West Grove, PA, <http://www.jacksonimmuno.com>). hFRPE (Lonza) cells were cultured initially in RtEGM media with supplements (Lonza) until the cells reached confluence, and then they were cultured in the iPSC serum-free media (for the metabolomic assay) or in DMEM/F12 + 2% FBS (for all other studies) similar to ARPE-19 cells (American Type Culture Collection; passages 20–25).

### RNA Analysis by Reverse-Transcription Polymerase Chain Reaction

Total RNA was isolated using QiaShredder and RNeasyPlus kits (both Qiagen, Hilden, Germany, <http://www1.qiagen.com>) as instructed. Reverse transcription was performed with 500 ng of total mRNA using a QuantiTect Reverse Transcription Kit (Qiagen) according to the manufacturer's recommendations. Twenty-five nanograms of cDNA was polymerase chain reaction (PCR)-amplified in Platinum PCR SuperMix (Invitrogen). Primer sequences used for detection of Nanog [24], Lin28 [29], tyrosinase [21], bestrophin [24], cellular retinaldehyde-binding protein (CRALBP) [25], retinal pigment epithelium-specific 65-kDa protein (RPE65) [24], and glyceraldehyde-3-phosphate dehydrogenase [25] were previously reported.

**Table 1.** Exogenous transcription factors and small molecules used in iPSC reprogramming

Clone	Source cells	Transcription factor(s)	Small molecules
4F-iPSC	Human fetal lung fibroblast cell line (IMR-90)	<i>OCT4</i> <i>SOX2</i> <i>NANOG</i> <i>LIN28</i>	
2F-iPSC-1	Human primary neonatal epidermal keratinocytes	<i>OCT4</i> <i>KLF4</i>	CHIR99021 Tranylcypromine
2F-iPSC-2	Human primary neonatal epidermal keratinocytes	<i>OCT4</i> <i>KLF4</i>	CHIR99021 SB431542 Tranylcypromine PD0325901
2F-iPSC-3	Human primary neonatal epidermal keratinocytes	<i>OCT4</i> <i>KLF4</i>	CHIR99021 SB431542 Tranylcypromine PD0325901
2F-iPSC-4	Human primary neonatal epidermal keratinocytes	<i>OCT4</i> <i>KLF4</i>	CHIR99021 SB431542 Tranylcypromine PD0325901
1F-iPSC-1	Human primary neonatal epidermal keratinocytes	<i>OCT4</i>	Sodium butyrate PS48 A83-01 PD0325901
1F-iPSC-2	Human primary neonatal epidermal keratinocytes	<i>OCT4</i>	Sodium butyrate PS48 A83-01 PD0325901
1F-iPSC-3	Human primary neonatal epidermal keratinocytes	<i>OCT4</i>	Sodium butyrate PS48 A83-01 PD0325901
1F-iPSC-4	Human primary neonatal epidermal keratinocytes	<i>OCT4</i>	Sodium butyrate PS48 A83-01 PD0325901

Several clones were generated from the same source material during reprogramming. These are numbered 1–4 for the 2F- and 1F-iPSCs. Abbreviations: 1F, one-factor; 2F, two-factor; 4F, four-factor; iPSC, induced pluripotent stem cell.

### Immunohistochemistry and Electron Microscopy

Cellular monolayers (containing cells that had not been expanded or passaged) were fixed with 4% paraformaldehyde (4°C overnight), manually detached, embedded in O.C.T. (Sakura Finetek, Torrance, CA, <http://www.sakura-americas.com>) and cryosectioned (16- $\mu$ m thickness). Monolayers were also stained within the plate for ZO-1, or after methanol/acetate fixation on Transwell membranes (Millipore, Billerica, MA, <http://www.millipore.com>) for rabbit pigment epithelium-derived factor (PEDF) (1:50; Santa Cruz Biotechnology Inc., Santa Cruz, CA, <http://www.scbt.com>) and mouse bestrophin (1:100; Novus, Littleton, CO, [www.novusbio.com](http://www.novusbio.com)). Immunohistochemistry on frozen samples was performed using primary antibodies raised against mouse monoclonal bestrophin, CRALBP (1:30; Abcam, Cambridge, MA, <http://www.abcam.com>), RPE65 (1:100; Novus), and ZO-1 (1:500; Invitrogen). Secondary antibodies, 4',6-diamidino-2-phenylindole (DAPI), and ToPro-3 were obtained from Invitrogen. Samples were mounted using Vectashield (Vector Laboratories, Burlingame, CA, <http://www.vectorlabs.com>) and imaged on a confocal fluorescence microscope (Carl Zeiss, Jena, Germany, <http://www.zeiss.com>).

For immunohistological analyses of RCS rat retinas with implanted 1F-iPS-RPE, enucleated eyes were fixed in 4% paraformaldehyde after removing the cornea and lens for 1 hour on ice. The retinas were then transferred to 30% sucrose in phosphate-buffered saline (PBS) and stored at 4°C overnight. The eyes were frozen in O.C.T. and sectioned in 12–14- $\mu$ m sections. Slides were briefly incubated with 2% normal goat serum before adding Recoverin antibodies (1:1,000; Millipore) for 2 hours (room temperature) and anti-rabbit secondary antibodies (1:1,000; Invitrogen) for 30 minutes (room temperature). For electron microscopy analyses, rats were exsanguinated with 0.9% saline and perfused with 4% paraformaldehyde, 1.5% gluteraldehyde, and 0.02% picric acid in 0.1 M cacodylate buffer. Enucleated eyes were halved close to the optic nerve and fixed for a prolonged period at 4°C. After being washed, the eyes were postfixed in 1% osmium tetroxide, dehydrated in a graded ethanol series, transitioned in propylene oxide, and embedded in LX112 resin (Ladd Research Industries, Williston, VT, <http://www.laddresearch.com>). Seventy-nanometer thin sections were cut with a diamond knife (Diatome, Hatfield PA, <http://www.diatomeknives.com>), mounted on copper slot grids precoated with parlodion, and

then stained with uranyl acetate and lead citrate. Imaging was performed on a Philips CM100 electron microscope (FEI, Hillsboro, OR, <http://www.fei.com>) at 80 kV and a Megaview III charge-coupled device camera (Olympus Soft Imaging Solutions, Lakewood CO).

### Enzyme-Linked Immunosorbent Assays

Low-passage (passages 2–4) 1F-iPS-RPE (1F-iPS-1, -2) and hRPE cells on Transwell membranes were maintained until they were postconfluent. Sandwich enzyme-linked immunosorbent assays (ELISAs) for human PEDF and vascular endothelial growth factor (VEGF) were performed using kits (Millipore and R&D Systems Inc. [Minneapolis, <http://www.rndsystems.com>], respectively) according to the manufacturers' instructions. Supernatant from the apical cell side (upper Transwell chamber) was used to detect secreted PEDF protein, and the basolateral supernatant from the same wells (lower Transwell chamber) was analyzed in the VEGF assay (each sample was analyzed in triplicate). The assays were performed three times with six replicate samples of each cell type (the most representative data were shown). The optical density readings were measured using a Synergy two-plate reader (BioTek Instruments, Inc., Winooski, VT, [www.biotek.com](http://www.biotek.com)).

### In-Cell Western Analyses

In-cell Western analyses were performed according to the manufacturer's instructions (LI-COR Biosciences, Lincoln, NE, <http://www.licor.com>) on all low-passage (passages 2–4) RPE cells (seeded on 96-well plates) simultaneously. Twenty-eight different antibodies were used in triplicate to obtain average protein expression levels. Goat antibodies against Sox2 (1:750; Santa Cruz Biotechnology) and Trp1 (1:50; Santa Cruz Biotechnology) were used. Mouse antibodies included vimentin (1:100; Millipore), Mitf (1:400; Exalpha, Shirley, MA, [www.exalpha.com](http://www.exalpha.com)), N-cadherin (1:200; BD Transduction, San Jose, CA, <http://bdbiosciences.com>), Na-K-ATPase (1:100; Abcam), occludin (1:100; Invitrogen), CD36 (1:100; Abcam), and IV $\beta$ 5 (1:100; Abcam). Rabbit antibodies included  $\beta$ -catenin (1:2,000; Sigma-Aldrich), cyclin D1 (1:100; Invitrogen), CK18 (1:100; Abcam), CK7 (1:100; Abcam), Ki67 (1:400; Abcam), MerTK (1:400; Novus), Otx2 (1:1,500; Chemicon), peropsin (1:100; Novus), phosphatase and tensin homolog (PTEN) (1:100; Cell Signaling), Tuj1 (1:1,000; Covance, Princeton, NJ, <http://www.covance.com>), tyrosinase (1:100; Novus), Wnt2b (1:100; Invitrogen), LAMP-1 (1:200; Abcam), and connexin 43 (1:50; Cell Signaling). Rat anti- $\beta$ -tubulin (1:1,000; Abcam) was used as a reference for which protein expression across the plates was normalized. IRDye 800 secondary antibodies were added (LI-COR Biosciences), and cell number differences were corrected by normalizing with Sapphire 700 (1:1,000; LI-COR Biosciences) and DRAQ5 (1:10,000; Cell Signaling). The plates were scanned individually on an Odyssey Infrared Imaging System (LI-COR Biosciences), and differences were plotted using Excel software (Microsoft, Redmond, WA, <http://www.microsoft.com>).

### Phagocytosis Assay

Photoreceptor outer segments (POSS) were isolated from fresh porcine eyes (Sierra for Medical Science, Whittier, CA, <http://www.sierra-medical.com>) as previously described [30] and labeled with fluorescein-5-isothiocyanate (FITC) (isomer I; Invitrogen) as recommended by the manufacturer. Protein concen-

tration was quantified using Bradford assays, and RPE cells were incubated with 10  $\mu$ g of total POS protein per cm<sup>2</sup> of cell culture area. At various time points, nonphagocytosed POSSs were removed by repeated vigorous washes with PBS, fixed with 4% paraformaldehyde, permeabilized with 1% Triton X-100, and DAPI stained. If indicated, FITC fluorescence was quenched with 0.2% Trypan Blue (Invitrogen) for 10 minutes before fixation. Samples were imaged on a fluorescence microscope.

### Metabolite Extraction Method

For the in vitro assays, low-passage (passages 2–4) cells grown in separate wells of 24-well plates were washed with PBS and released from the plate surfaces by scraping. Then,  $5.0 \times 10^5$  cells were pelleted and frozen so that the extraction and liquid chromatography/mass spectrometry (LC/MS) analysis could be performed on all the cell types simultaneously. Three hundred microliters of hot (80°C) methanol (100%) was added, vortexed (30 seconds), and incubated for 1–2 minutes at 80°C before centrifugation (15 minutes, 13,000 rpm, 4°C). The same process was repeated with the precipitate. Supernatants (~600  $\mu$ l total) were pooled and the dried with a vacuum concentrator (Speed-Vac; Thermo Fisher, Pittsburg, PA, <http://www.fishersci.com>). The sample was redissolved in 150  $\mu$ l of 10% MeOH/90% water 5 mM ammonium acetate and centrifuged (10 minutes, 13,000 rpm).

### LC/MS Analysis

Analyses were performed using a high-performance liquid chromatography (HPLC) system (1200 series; Agilent Technologies, Palo Alto, CA, <http://www.agilent.com>) coupled to a 6,538 UHD Accurate-Mass quadrupole time-of-flight (Q-TOF) (Agilent Technologies) operated in positive electrospray ionization (ESI+) mode. Vials containing extracted metabolites were kept at  $-20^{\circ}\text{C}$  prior to LC/MS analysis. Cell population extractions were separated using a  $150 \times 0.5$  mm (diameter) Zorbax C18 columns (Agilent, Santa Clara, CA, <http://www.agilent.com>) with 5- $\mu$ m particles, at a flow rate of 20  $\mu$ l/minute. For the in vitro assay, the instrument was operated using the following solvent system: A = 0.1% formic acid in water and B = 0.1% formic acid in acetonitrile. The gradient elution used started at 100% A (time, 0–5 minutes) and finished at 100% B (35–40 minutes). The injection volume was 8  $\mu$ l. ESI conditions were as follows: gas temperature, 325°C; drying gas, 11 L/minute; nebulizer, 30 pound-force per square inch gauge; fragmentor, 120 V; and skimmer, 65 V. For the in vivo assay, the gradient elution used started with 100% A (injection) at 0 minutes, increased to 80% A at 5 minutes, and reached 100% B at 43 minutes; the organic phase (B) then slowly went down to 98% at 43–55 minutes and then quickly went to 95% A at 60 minutes. The instrument was set to acquire over the m/z range 80–1,000 (in vitro assay) or 80–1,500 (in vivo assay) with an acquisition rate of 1.3 spectra/second. The MS/MS for each selected sample were repeated three times at three collision energies: 20 V, 60 V, and a slope of  $5 \times (M/100) + 5$ , where M denotes the molecular weight of selected precursor. All pure standards, formic acid, and acetic acid were purchased from Sigma-Aldrich, except lysophosphatidylethanolamine (LysoPE) standard (phosphatidylethanolamine PE 18:0) from Avanti Polar Lipids, Inc. (Alabaster, AL, <http://www.avantilipids.com>). LC/MS-grade methanol, acetonitrile, and water were purchased from J.T. Baker (Phillipsburg, NJ, <http://www.avantormaterials.com>).



For the *in vitro* assay, the number of metabolic features dysregulated by at least twofold with a statistical significance of  $\leq 0.001$  were counted and compared with the total number of features identified to generate percentage values, which were plotted using Excel software.

For the *in vivo* assay, metabolites from snap-frozen eyes were extracted using methanol/chloroform/water/acetic acid mixture at a ratio of 60:25:14:1 (vol/vol/vol/vol), homogenized, and ground briefly with a pestle. Ice-cold methanol-based extraction solvent (200  $\mu$ l) was added, and the samples were ground for another minute before subjecting them to two rounds of homogenization with 600 and 400  $\mu$ l of extraction solvents; the samples were then flash frozen. Homogenates were thawed and centrifuged (10 minutes, 13,000 rpm), and 400  $\mu$ l of chilled acetonitrile (ACN) was added to extract the pellet twice. The pooled supernatants were dried down using a Speed-Vac without heating and eluted in ACN/water 1:0.8 (vol/vol) containing 5% MeOH, 5% chloroform, and 0.1% formic acid (in volume ratio). The HPLC separation of A2E and isoA2E and the MS/MS spectra of synthetic and endogenous A2E have been previously reported [31, 32]. A2E was synthesized as previously described [31] from ethanolamine and all-*trans*-retinal. Briefly, a mixture of all-*trans*-retinal (25 mg, 88  $\mu$ mol) and ethanolamine (3  $\mu$ l, >99% 38.7  $\mu$ mol, product number 398136; Sigma-Aldrich) in ethanol (EtOH) (1.0 ml) was stirred in the presence of acetic acid (3  $\mu$ l, 52  $\mu$ mol) at room temperature with a sealed cap in the dark for 3 days. After the mixture was concentrated *in vacuo*, the residue was purified by silica gel column chromatography. The synthetic A2E was dissolved in ACN:H<sub>2</sub>O:EtOH = 1:0.8:0.05 (vol/vol) for LC/MS analysis.

### Data Processing

LC/MS data from the retina extractions were processed by using XCMS online software (<http://metlin.scripps.edu/xcms/>) [33] online to detect and align features. XCMS analysis of these data provided a matrix containing the retention time, m/z value, and intensity of each feature for every extraction method discussed above. Each row in the matrix represented a feature. It is important to note that whereas the retention time and m/z values for each feature were consistent among extraction methods, the intensities of the features varied. By using the statistical "R" algorithm in XCMS, each row of feature intensities was normalized such that the highest value was 1. A two-dimensional representation of this matrix was calculated using multidimensional scaling as implemented within the software R. Standards were manually quantified by extracting ion chromatograms and integrating peak intensities with a Qualitative Analysis of Mass-Hunter Workstation (Agilent Technologies).

### RCS Rat Subretinal Injections

All animals used in these studies were treated in adherence to the NIH *Guide for the Care and Use of Laboratory Animals*. Low-passage (passages 2–4) differentiated iPS-RPE were harvested and transiently labeled with 25  $\mu$ M CellTracker Green CMFDA (Invitrogen) for 30 minutes at 37°C prior to injection. Roughly 100,000 cells in suspension were injected into the subretinal space of 3-week-old RCS albino rats' eyes ( $n = 45$ ) with a blunt 33-gauge Hamilton syringe (Hamilton, Reno, NV, <http://www.hamiltoncompany.com>) using a transscleral route, entering at the limbus and through the diametrically opposed retina. The fundi of the rats were visualized using confocal scanning

laser ophthalmoscopy (cSLO) (Heidelberg), and green fluorescence was used to identify the injection site; retinal detachments induced by the injections were imaged using optical coherence tomography (Heidelberg Engineering, Heidelberg, Germany, <http://www.heidelbergengineering.com>). The injected and control eyes were monitored at 4 ( $n = 8$ ), 5 ( $n = 8$ ), 6 ( $n = 10$ ), 12 ( $n = 10$ ), 18 ( $n = 4$ ), and 24 ( $n = 3$ ) weeks postinjection using cSLO and optical coherence tomography. Six weeks postinjection, rows of outer nuclear layer (ONL) cells were counted from images of histological preparations from four control and four 1F-iPS-RPE (1F-iPS-2) at roughly 1.5 mm from the optic nerve. In injected eyes, only the regions where exogenous pigmented cells were observed in the RPE layer were examined. Retinal thickness measurements were made by semiautomatically drawing segmentation lines on Heidelberg optical coherence tomography images that flanked the edge of the inner retina and the tip of the POS. From each image, three maximal thickness measurements were recorded and averaged. For iPS-RPE injected eyes, the measurements were made from regions where RPE cells incorporated on the basis of pigmentation observed in fundus images. The results were plotted using Excel software.

### Focal Electroretinography

Focal electroretinography (fERG) recordings were measured using a Micron III platform (Phoenix Research Laboratories, Pleasanton, CA, <http://phoenixreslabs.com>) in parallel with an Epsilon electroretinography (ERG) device (Diagnosys LLC, Lowell, MA, <http://www.diagnosyllc.com>). Dark-adapted (12 hours) rats were anesthetized under dim red light with intraperitoneal delivery of 15 mg/kg body weight (BW) ketamine and 7 mg/kg BW xylazine and placed on a heating pad that maintained their body temperature at 35–36°C throughout the experiment. The pupils were dilated with a mixed solution of 1% tropicamide and 2.5% phenylephrine. Recordings were measured from a corneal electrode attached to the Micron III camera lens. One needle probe was inserted for the reference subcutaneously between the eyes and a grounding probe was inserted into the base of the tail. Then 12.6 million lux of light from an LED source projector was injected into a spot area (roughly 250  $\mu$ m diameter, 0.7% of a 6.1-mm full-size radius rat retina) in a 30-ms pulse width over the 1F-RPE injected region, uninjected region in the same eye, the contralateral eye, and in eyes injected with PBS. Fundus images were captured after the recordings in each eye were completed. Twenty traces were obtained and averaged for each area examined. The amplitude of the b-wave was measured from the trough to the peak of the first visible wave. In wild-type animals, we recorded impulses beginning at 0.3 cd-second/m<sup>2</sup> that doubled in intensity until reaching 10,000 cd-second/m<sup>2</sup> (supplemental online Fig. 10).

## RESULTS

We recently described new methods to efficiently generate human iPSCs with only one or two of the conventionally used four transcription factors and treatment with small molecules [13, 14]. These naïve iPSCs expressed key pluripotency markers and formed teratomas *in vivo*. Whether these iPSCs possess full differentiation capabilities that match conventionally derived iPSCs has not been evaluated. In this study, we assessed the differentiation potential of one- and two-factor-derived iPSCs in comparison with conventional four-factor-derived iPSCs.

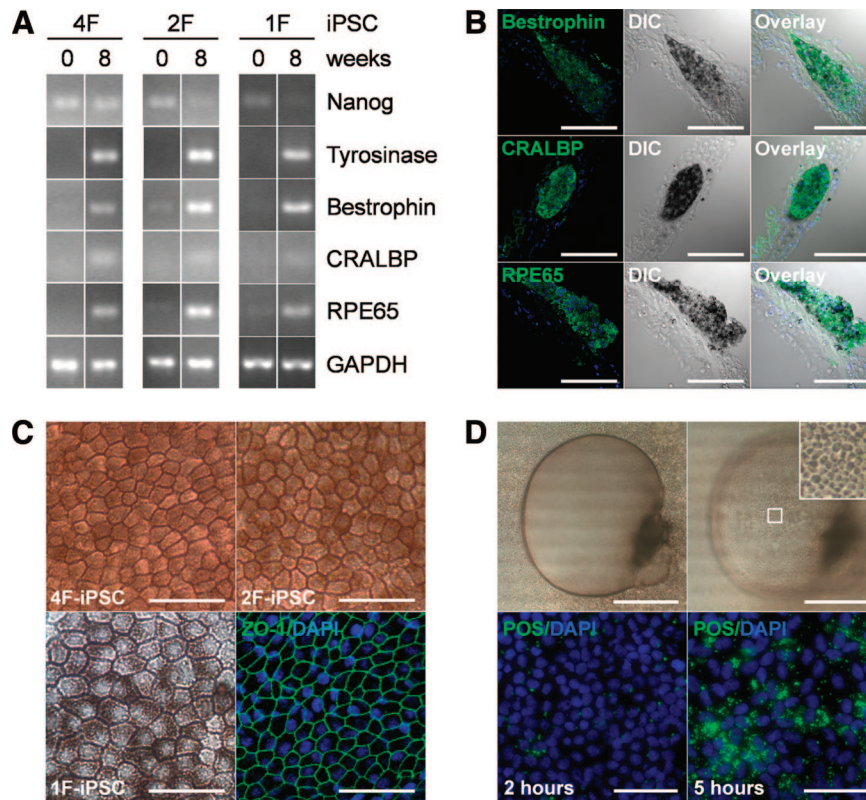


**Figure 1.** (A): mRNA expression was analyzed in 4F-, 2F-, and 1F-iPSCs at the beginning and end of 8 weeks of directed differentiation. Expression of the pluripotency marker Nanog decreased with differentiation but remained detectable in 4F-iPSCs that were transfected with Nanog during reprogramming. Expression of the melanogenesis marker tyrosinase was induced during differentiation, and its expression correlated closely with development of cellular pigmentation. RPE terminal differentiation markers bestrophin, CRALBP, and RPE65 were minimally expressed in undifferentiated iPSCs but strongly expressed in differentiated cells. GAPDH served as loading control. (B): Immunohistochemical analysis of differentiated 4F-, 2F-, and 1F-iPS-RPE confirmed protein expression of terminal RPE differentiation markers and a clear localization in cells also expressing pigment (representative results of 2F-iPS-RPE shown). (C): Isolation and expansion of pigmented cell clusters from differentiated 4F-, 2F-, and 1F-iPS-RPE yielded homogenous cultures of cells with morphological features characteristic of RPE cells, such as monolayer growth, hexagonal shape, and pronounced pigmentation. Expression and localization of the tight junction protein ZO-1 was detectable in 4F-, 2F-, and 1F-iPS-RPE (representative results of 4F-iPS-RPE shown). (D): iPS-RPE exhibited RPE functionality in vitro including directional fluid transport and photoreceptor outer segment (POS) phagocytosis. Barrier properties of the cellular monolayer in combination with apical-to-basolateral fluid transport resulted in progressive formation of fluid-filled domes in 4F-, 2F-, and 1F-iPS-RPE cultures (top panels, representative results of 4F-iPS-RPE). Furthermore, POS phagocytosis was detectable in 4F-, 2F-, and 1F-iPS-RPE (bottom panels, representative results of 2F-iPS-RPE). Two hours after addition of fluorescein-5-isothiocyanate-labeled POS to iPS-RPE cultures, the POS were bound but not yet internalized. The increase in detectable POS after 5 hours represents POS internalization. Scale bars = 100  $\mu\text{m}$  (B), 50  $\mu\text{m}$  (C), 1000  $\mu\text{m}$  (D, top), and 50  $\mu\text{m}$  (D, bottom). Abbreviations: 1F, one-factor; 2F, two-factor; 4F, four-factor; DAPI, 4',6-diamidino-2-phenylindole; DIC, Differential interference contrast; GAPDH, glyceraldehyde-3-phosphate dehydrogenase; iPSC, induced pluripotent stem cell; RPE, retinal pigment epithelium.

We subjected one conventionally reprogrammed iPSC clone (4F-iPSCs), four different clonal lines of iPSCs generated by using two reprogramming factors (2F-iPSCs), and four clonal lines of one-factor-derived iPSCs (1F-iPSCs) to either published spontaneous or directed differentiation protocols [20]. (The reagents used for reprogramming are listed in Table 1.) Directed differentiation resulted in more rapid and efficient generation of pigmented cells (6 weeks; technique depicted in supplemental online Fig. 1). Pigmentation in embryonic RPE cells is observed in a similar time frame in vivo [34]. Although differentiating iPSC cultures demonstrated a decrease in expression of the pluripotency marker Nanog, expression of the melanogenesis marker tyrosinase and the RPE terminal differentiation markers bestrophin, CRALBP, and RPE65 increased (Fig. 1A; supplemental online Fig. 2). These results are similar to those observed when RPE cells are differentiated from conventional iPSCs [22–26]. Immunohistochemical analysis revealed a close colocalization of terminal dif-

ferentiation marker expression and cellular pigment formation (Fig. 1B; supplemental online Fig. 3). When these pigmented cell clusters were isolated and replated, they expanded as homogeneous monolayers of cells with characteristic RPE polygonal morphology, dense pigmentation, and ZO-1-positive intercellular tight junctions (Fig. 1C).

To use iPSC-derived RPE as autologous grafts to replace aged and dysfunctional RPE cells in diseases such as AMD, these cells need to perform essential RPE functions such as apical-to-basolateral fluid transport, barrier formation, and phagocytosis of POSs. The RPE monolayer in vivo forms a tight barrier between the retina on its apical side and the choroidal circulation on its basolateral side (outer blood-retinal barrier); RPE cells constantly pump fluid from the apical (retinal) to the basolateral (choroidal) side. For functional RPE cells in vitro, these two characteristics have been shown to result in the accumulation of fluid under the cell monolayer, leading to the formation of fluid-filled

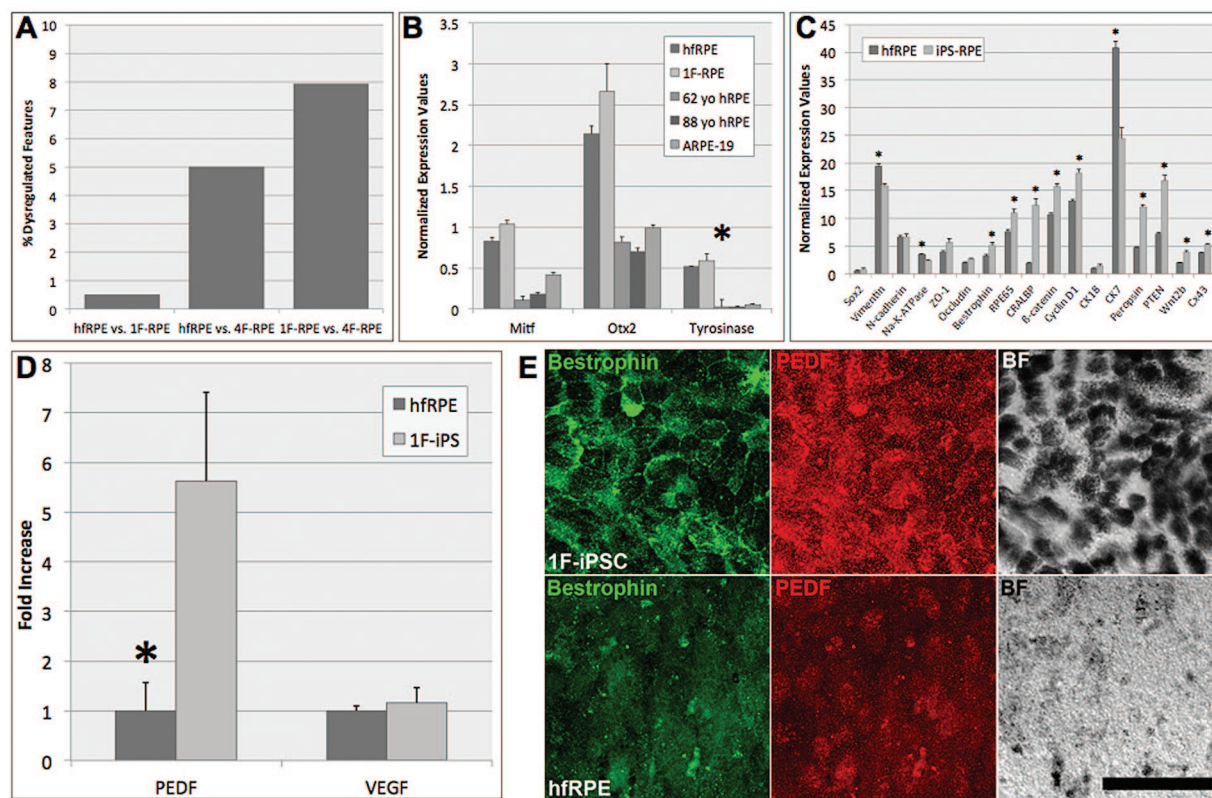


**Figure 2.** (A): The percentage of dysregulated metabolic features (fold change  $\geq 2$  with high statistical significance,  $p \leq 0.001$ ) was compared between hRPE, 1F-iPSC-RPE (1F-iPSC-2), and 4F-iPSC-RPE. Nominal disparities were observed between hRPE and 1F-iPSC-RPE (0.5%; 82 of 15,651 total features). A 10-fold higher percentage of dysregulated features was observed between hRPE and 4F-RPE although the overall difference was still low (5.0%; 691 of 13,853 total features). Few differences were observed between 1F-iPSC-RPE and 4F-iPSC-RPE (7.9%; 1,320 of 16,682 total features); however, both 1F and 4F seemed to be more similar to hRPE than each other. (B): In-cell Western analyses comparing normalized protein expression values between hRPE, 1F-iPSC-RPE (1F-iPSC-2), 4F-iPSC-RPE, 62-year-old hRPE, 88-year-old hRPE, and ARPE-19 cells revealed differences in expression levels of Mitf, Otx2, and tyrosinase. hRPE and 1F-iPSC-RPE were consistently the most similar of all the cell types examined. One-way analysis of variance tests revealed that the differences in tyrosinase expression between the groups were statistically significant ( $p = .2$ ). (C): Direct comparison of the normalized expression values collected from the in-cell Western analysis in hRPE and 1F-iPSC-RPE for the proteins listed on the x-axis. (D): A quantitative comparison of PEDF and VEGF secretion by hRPE and 1F-iPSC-RPE (1F-iPSC-2) cells was performed using sandwich enzyme-linked immunosorbent assays. The results were plotted as fold increase above hRPE levels. A 5.6-fold ( $p = .019$ ) difference in secreted PEDF was detected between the hRPE and 1F-iPSC-RPE. No significant difference in secreted VEGF was detected (1.2-fold,  $p = .68$ ) between the two cell types. (E): Immunocytochemistry was performed on 1F-iPSC-2 and hRPE grown on Transwell filters. Bestrophin labeling (green) in 1F-iPSC-RPE staining marks the well-defined basolateral cell membranes but was diffusely expressed in hRPE. PEDF (red) was more readily detectable in 1F-iPSC-RPE than hRPE, and much more pigment was synthesized in 1F-iPSC-RPE cultures than in hRPE, as observed in the BF images. Collectively, these observations demonstrate that 1F-iPSC-RPE cells strongly resemble hRPE but are in an advanced differentiation state. Errors bars in all panels represent SEM values. Scale bar = 50  $\mu\text{m}$  (E). Abbreviations: 1F, one-factor; 4F, four-factor; BF, bright field; hRPE, human fetal retinal pigment epithelium; hRPE, human retinal pigment epithelium; iPSC, induced pluripotent stem; iPSC, induced pluripotent stem cell; RPE, retinal pigment epithelium; VEGF, vascular endothelial growth factor; yo, year old.

cellular domes [35]. We consistently observed this phenomenon in all cultures of iPSC-RPE cells, demonstrating cellular barrier formation and directional apical-to-basolateral fluid transport (Fig. 1D). Another RPE-specific function *in vivo* is the phagocytosis and degradation of shed POSs [36]. When we challenged iPSC-RPE cells with isolated POSs, we indeed detected pronounced phagocytosis activity (Fig. 1D).

To more closely determine how iPSC-RPE and hRPE functionality correlates, we compared the metabolomes of these cell types. The metabolomes of keratinocytes and fibroblasts, naïve stem cells, and differentiated RPE were analyzed with a novel and high-resolution approach using LC coupled to ESI Q-TOF MS. Our MS-based platform enabled us to detect thousands of me-

tabolite features, defined as molecular entities with a unique mass/charge and retention time value. When directly compared, the percentage of dysregulated features between populations can be used to correlatively determine how similarly they function biochemically. The largest disparities were observed between naïve 4F- and 1F-iPSCs and the fetal fibroblasts and neonatal keratinocytes lines from which they were reprogrammed. Remarkably, few differences were observed when comparing the naïve 4F- and 1F-iPSCs with hESCs (and between themselves), even though they originated from different cell types at different developmental stages. Importantly, few metabolic differences (0.5%) were also observed between 1F-iPSC-RPE and hRPE (Fig. 2A). 4F-iPSC-RPE and hRPE also differed only slightly



(5.0%), but this difference was 10-fold higher than that observed between 1F-iPS-RPE and hRPE. Furthermore, the differences between 1F- and 4F-iPS-RPE were low (7.9%), but higher than when either sample was compared with hRPE.

Furthermore, antibody-based in-cell Western proteomic analyses revealed that 1F-iPS-RPE and hRPE share far more similarities than 1F-iPS-RPE and aged primary hRPE cells do. Protein expression in hRPE, 1F-iPS-RPE, primary adult hRPE cells (from 62- and 88-year-old donors), and the ARPE-19 cultures was examined using 28 known protein markers of RPE development and terminal differentiation. One-way analysis of variance (ANOVA) tests revealed, with few exceptions, that expression levels of the markers chosen were not statistically different. Exceptions included markers of advanced differentiation RPE65 ( $p = .02$ ), tyrosinase ( $p = .04$ ), and connexin 43 (Cx43;  $p = .002$ ). Closer analyses revealed that the expression levels of the markers examined in 1F-iPS-RPE consistently correlated best with hRPE (Fig. 2B). Interestingly, when 1F-iPS-RPE and hRPE were directly compared, significant differences were observed in the expression of terminal differentiation markers, including bestrophin ( $p = .02$ ), RPE65 ( $p = .05$ ), CRALBP ( $p = .01$ ), peropsin ( $p = .003$ ), and Cx43 ( $p = .02$ ) (Fig. 2C).

ELISAs were used to quantify the amount of secreted PEDF and VEGF from 1F-iPS-RPE and hRPE because these factors have been implicated as modulators of choroidal neovascularization in AMD [37]. Although no significant difference was observed in the amount of VEGF secreted by 1F-iPS-RPE and hRPE ( $p = .68$ ), the amount of PEDF secreted by 1F-iPS-RPE was substantially higher (5.6-fold;  $p = .02$ ) than that secreted by hRPE (Fig. 2D). This result is significant since increased PEDF may reflect an advanced differentiation status [38, 39]. Additionally, the expression of bestrophin in 1F-iPS-RPE was localized to the basolateral membranes but diffusely expressed in hRPE, and the 1F-iPS-RPE synthesized much more melanin pigment than hRPE did (Fig. 2E).

We next examined whether 1F-iPS-RPE can prevent photoreceptor death *in vivo* using a rat model of RPE-mediated retinal degeneration, the Royal College of Surgeons (RCS) rat. Retinal degeneration in this strain is complete and rapid since the RPE cells cannot phagocytose POSs. We injected 1F-iPS-RPE into the subretinal space of albino RCS rat retinas using a novel technique after transiently labeling the cells with fluorescent CellTracker and immediately imaging the retina *in vivo* to determine the efficacy of the injection. To facilitate *in vivo* monitoring we used cSLO, fundus autofluorescence, and optical coherence tomography imaging. Transient CellTracker labeling avoids the risk of altering gene expression or cellular functions, problems sometimes observed after introducing transgenic markers, such as green fluorescent protein (supplemental online Fig. 5A). To demonstrate that 1F-iPS-RPE cells are functional *in vivo* after transplantation in RCS rats, we monitored autofluorescence as a biomarker of active RPE phagocytosis and visual cycling. Normally, the fundus of the retina exhibits uniform fluorescence, but in human cases of sensory retina and RPE atrophy, profoundly reduced fluorescence is observed [40, 41]. At the margins of the degenerating regions, however, elevated autofluorescence is often detected [40]; these signals may correlate with early-stage RPE dysfunction (impaired phagocytosis) and buildup of degenerating photoreceptor outer segments in a debris layer similar to that observed in the RCS rat [42]. In fact, a thick autofluorescent debris layer is observed in human cases of retinal degeneration

linked to a mutation in the MerTK gene [43], the same gene mutated as in RCS rats.

We determined after careful analyses of cryosectioned RCS rat retinas that detectable autofluorescent patterns differed in regions where 1F-iPS-RPE cells were transplanted. In uninjected animals, the autofluorescent layer was more thick and diffuse, occupying the entire subretinal space and debris layer (Fig. 3A, arrows). In regions implanted with 1F-iPS-RPE, however, the autofluorescence was detected in a restricted and punctate pattern in the RPE cell layer (Fig. 3B, arrows; Fig. 4D), demonstrating very efficient delivery and incorporation of the 1F-iPS-RPE cells. Remarkably, the implanted 1F-iPS-RPE cells could also be visualized 1.4 years after implantation (Fig. 3C). To examine the ultrastructural features of the implanted cells and their spatial orientation in relation to Bruch's membrane and the outer retina, we used electron microscopy. Examinations performed 7 months after transplantation revealed that the 1F-iPS-RPE (easily identifiable as pigmented cells in albino animals) were perfectly polarized in normal proximity to Bruch's membrane and correctly extended apical processes toward the photoreceptor cells (Fig. 3D). Similar findings were observed 1.4 years after implantation (Fig. 3E), and we discovered that at this age the implanted cells were also easily identifiable (and functional) since they had phagocytosed large amounts of debris from the subretinal space (Fig. 3F, arrows). On the basis of our analyses, the majority of the transplanted cells, despite being injected as a bolus, incorporated as a monolayer into the RPE cell layer. We did observe occasional instances where the RPE cells existed in multilayered aggregates (supplemental online Fig. 8). However, it is very encouraging that the 1F-iPS-RPE appeared, overall, to integrate very efficiently into the correct cell layer after transplantation after such a simple experimental delivery.

We speculated that the large amount of debris phagocytosed by the implanted cells contributed to the bright autofluorescence we observed previously. The dominant fundus fluorophore is RPE lipofuscin [44], and the major RPE lipofuscin fluorophore is A2E [45], a nondegradable pyridinium bisretinoid probably generated in photoreceptor outer segments that accumulates in the RPE after phagocytosis [46]. Bisretinoid biosynthesis is significantly enhanced in the RCS rat because of improper clearance of outer segments [42]. We confirmed rapid accumulation of A2E in RCS rat retinas using mass spectrometry over several developmental time points concurrent with photoreceptors degradation (Fig. 4A). The mass spectrometry signal intensity of A2E increased 3.9-fold between 3 and 10 weeks (289,115–1,122,397) but was significantly reduced 8 (66.9%) and 10 (71.2%) weeks after 1F-iPS-RPE injection (11 and 13 weeks old, respectively) (Fig. 4B; mass spectrometry data shown in supplemental online Fig. 6). These data suggest that transplanted 1F-iPS-RPE cells phagocytose much of the debris before A2E can be formed. Autofluorescent lipofuscin can be directly visualized using fluorescent microscopy on frozen sections of RCS rat retinas. In uninjected eyes, nominal autofluorescence and recoverin immunoreactivity was observed in RPE cells (Fig. 4C, bracket). Conversely, in 1F-iPS-RPE injected eyes, intense autofluorescence was observed in the RPE cell layer (Fig. 4D, bracket). These data strongly suggest that the transplanted 1F-iPS-RPE cells are functional and are phagocytosing outer segments from the debris layer. In fact, using electron microscopy, we detected large



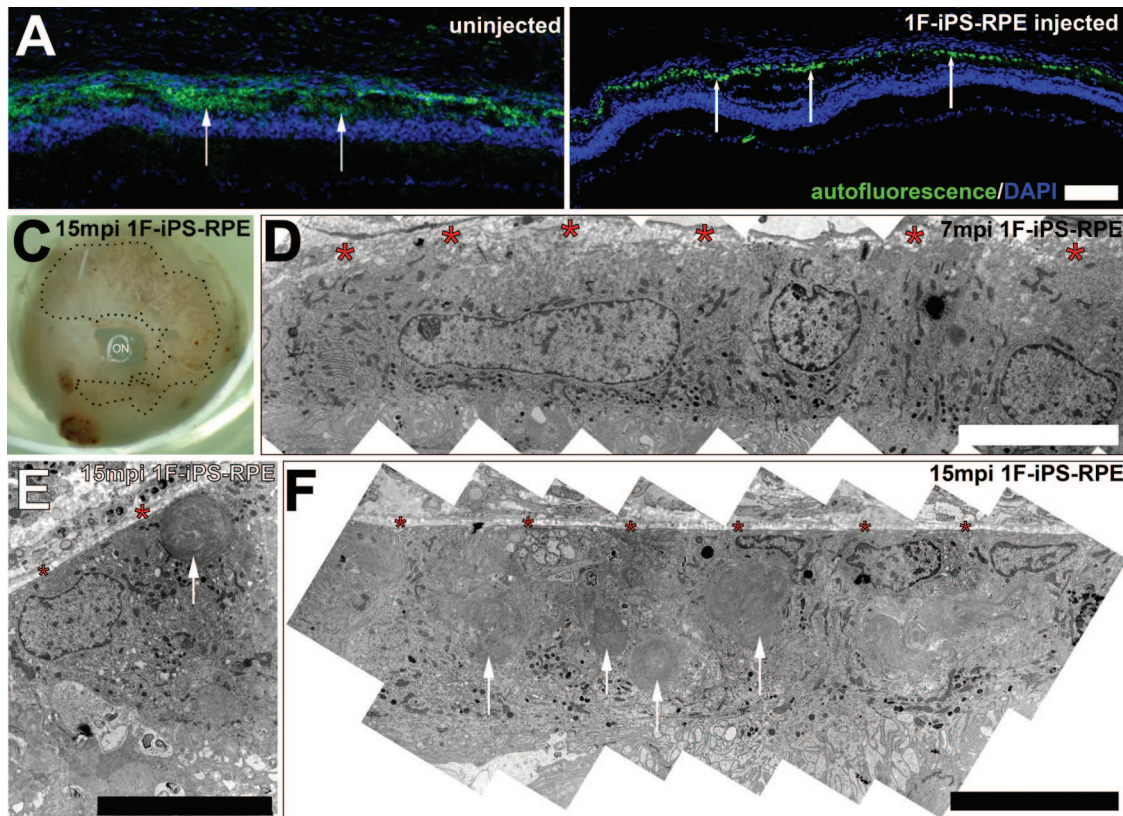


**Figure 3.** (A): Autofluorescence in uninjected Royal College of Surgeons (RCS) rat eyes was detected in a broad diffuse region correlating with the subretinal space. (B): In contralateral eyes injected with 1F-iPS-RPE (1F-iPS-2), the autofluorescence pattern was punctate and limited to the RPE cell layer. (C): Implanted pigmented 1F-iPS-RPE cells could be observed in albino RCS rat eyes after enucleation. (D): The implanted 1F-iPS-RPE cells incorporated into the RPE layer and were correctly polarized. Red asterisks mark Bruch's membrane. (E, F): Implanted cells could also be detected 15 months after implantation. Arrows point to debris accumulation in the implanted 1F-iPS-RPE cells. Scale bars = 100  $\mu\text{m}$  (A, B) and 10  $\mu\text{m}$  (D–F). Abbreviations: 1F, one-factor; iPS, induced pluripotent stem; mpi, months postinjection; RPE, retinal pigment epithelium.

amounts of debris highly resembling photoreceptor outer segments only in implanted 1F-iPS-RPE cells 7 months after transplantation (Fig. 4E, blue). Other subcellular materials were detected only in implanted 1F-iPS-RPE, including lipofuscin (Fig. 4F, green) and extracellular deposits (Fig. 4G, red), known byproducts of photoreceptor outer segment phagocytosis 15 months after transplantation. At this stage, the host RPE cells (which are unable to phagocytose photoreceptor outer segments) were much smaller and did not contain debris (Fig. 4H), whereas the implanted 1F-iPS-RPE (Fig. 4I) were much larger. Additionally, since retinal macrophages are known to contribute to clearance of the debris layer in RCS rats [47–49], we looked for cells with macrophage features and morphologies in the sections. These were observed very sporadically in the subretinal space of the prepared sections (Fig. 4J), suggesting that the implanted 1F-iPS-RPE cells were primarily responsible for clearance of the debris layer.

The accumulation of lipofuscin in 1F-iPS-RPE cells may also indicate that the visual cycle is functional in transplanted RPE and host photoreceptor units. In mice with defective visual cycles (*RPE65* mutants), lipofuscin levels are reduced >90% [50] since the retinas from which A2E are generated are not manufactured [51]. Although retinal levels dropped rapidly in RCS rat eyes at time points consistent with photoreceptor degradation, in 1F-iPS-RPE transplanted eyes, retinal levels were significantly elevated 8 and 10 weeks postinjection ( $1.74\times$  and  $1.69\times$ , re-

spectively; supplemental online Fig. 7). Consequently, detection of retinal and lipofuscin in transplanted RPE cells likely indicates that the transplanted RPE cells integrated with the host photoreceptors and proceeded to phagocytose outer segments and recycle retinal in the visual cycle, demonstrating functional rescue.

We performed histological examinations 6 weeks after 1F-iPS-RPE injection to monitor the extent of anatomical rescue. These examinations revealed that a significantly higher number of rows of photoreceptor cell nuclei were observed in the ONL in RCS rat retinas injected with 1F-iPS-RPE as compared with untreated control animals (8.5-fold;  $p < .001$ ;  $n = 4$ ; Fig. 5A), demonstrating that 1F-iPS-RPE protected photoreceptors from degeneration in the RCS line. High-resolution novel *in vivo* imaging techniques were used for longitudinal tracking of the status of the retinal degeneration in transplanted animals. Retinal degeneration was quantified by measuring the thickness of the neurosensory retina. Reduced thickness in degenerating retinas corresponds to the loss of rows of photoreceptors in the ONL [52]. Significantly increased retinal thicknesses of 1F-iPS-RPE injected RCS rat retinas were observed at 4, 5, 6, 12, and 18 weeks after injection compared with age-matched untreated or sham-injected controls (Fig. 5B; supplemental online Fig. 9). By 6 months after injection, differences in retinal thickness in animals injected with iPS-RPE compared with controls were no longer statistically significant. These findings are comparable to those reported by



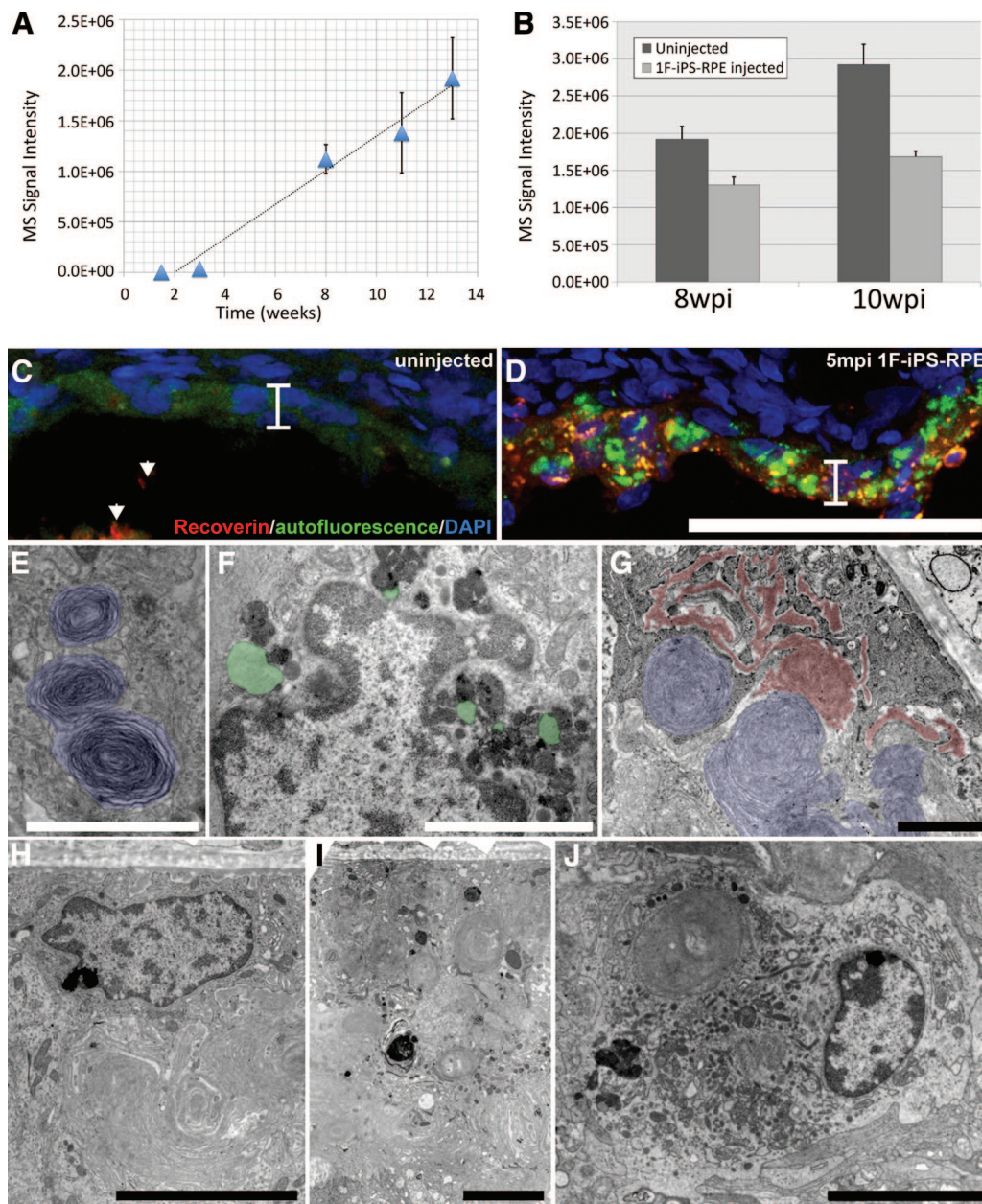


**Figure 4.** 1F-iPS-RPE (clone 1F-iPS-2) phagocytosed photoreceptor outer segment debris and reduced the levels of A2E accumulation in Royal College of Surgeons (RCS) rat eyes. **(A):** A2E accumulation in RCS rat as detected by liquid chromatography-mass spectrometry. **(B):** At 8 ( $n = 10$ ) and 10 ( $n = 6$ ) wpi with 1F-iPS-RPE, the injected eyes accumulated less A2E (66.9%,  $p = .03$ , and 71.2%,  $p = .006$  respectively). **(C):** In uninjected RCS rat eyes, nominal and diffuse autofluorescence and no recoverin (arrowheads) was detected in RPE cells. **(D):** Conversely, granular and highly autofluorescent lipofuscin and recoverin-positive material was detected in the RCS rat eyes after 1F-iPS-RPE cell implantation (the RPE monolayer is marked with a bracket [C, D]). **(E):** 1F-iPS-RPE phagocytosed material morphologically resembling photoreceptor outer segments 7 mpi. **(F, G):** 15 mpi, what appeared to be lipofuscin (green) and extracellular deposits (red) accumulated in 1F-iPS-RPE cells. **(H–J):** Host RPE **(H)**, implanted 1F-iPS-RPE **(I)**, and a host macrophage **(J)**. Scale bars = 50  $\mu\text{m}$  **(C, D)**, 2  $\mu\text{m}$  in **(E–G)**, and 5  $\mu\text{m}$  **(H–J)**. Abbreviations: 1F, one-factor; DAPI, 4',6-diamidino-2-phenylindole; iPS, induced pluripotent stem; mpi, months postinjection; MS, mass spectrometry; RPE, retinal pigment epithelium; wpi, weeks postinjection.

other groups using hES- or four-factor iPSC-derived RPE [20, 21, 23]. We also used optical coherence tomography imaging techniques to obtain spatial maps of retinal thickness around the injection area after 1F-iPS-RPE injections. These novel analyses revealed that the thickest regions of the retina correlated with the regions where transplanted pigmented RPE cells were present (Fig. 5C). Since the thickness is measured between the inner surface of the retina and photoreceptor outer segments, the

increases in thickness values were not due to increased layers of transplanted RPE cells. Importantly, tumor formation was not observed in any rat eye successfully injected with 1F-iPS-RPE at any time point up to 1.4 years after injection ( $n = 56$ ).

We performed novel image-guided fERG to determine whether the photoreceptors rescued by iPS-RPE injection in the RCS rats are functionally active. Conventional attempts to directly measure electrical activity of the retina using whole-field

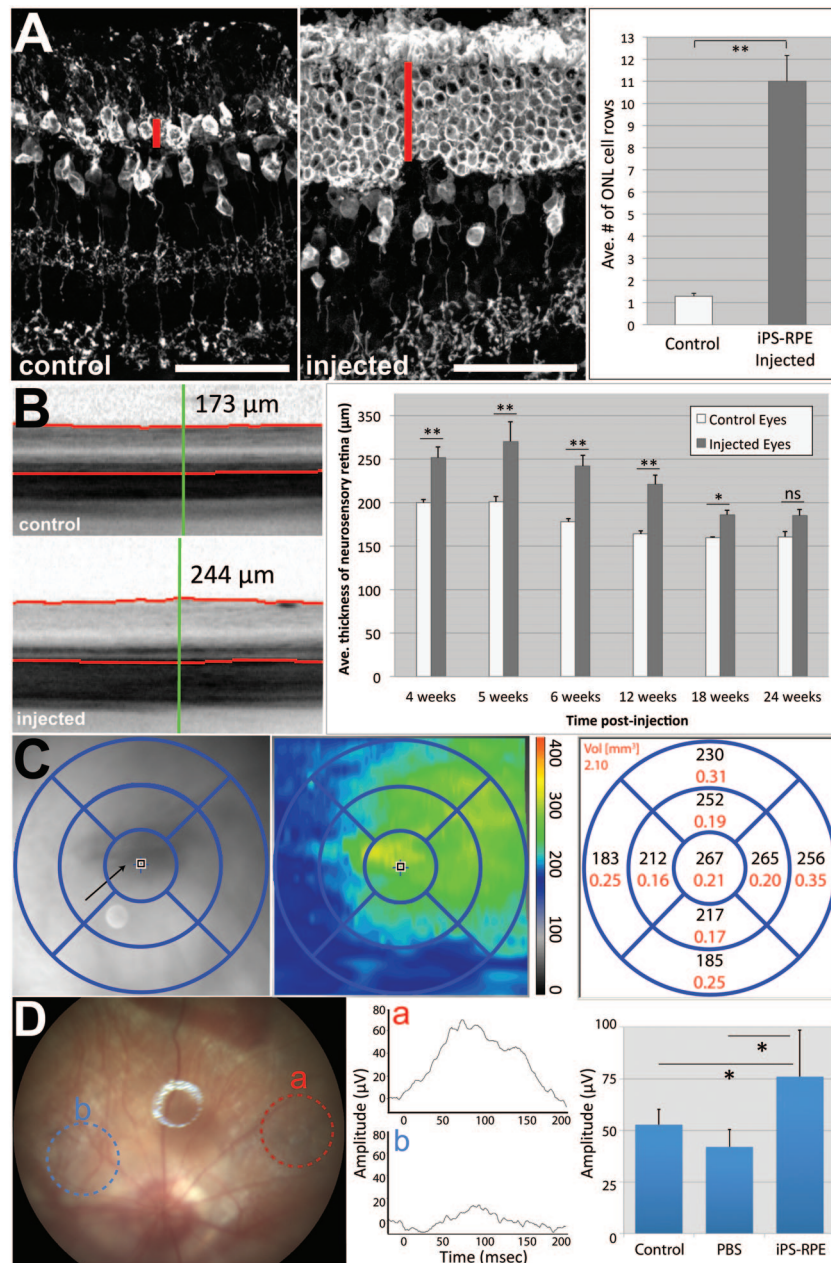


**Figure 5.** (A): Immunohistochemistry analyses were performed 6 weeks after transplantation of 1F-iPS-RPE (clone 1F-iPSC-2) in the subretinal space of RCS rats. Recoverin staining labeled photoreceptors (marked with a red line) and some bipolar cells. Note that at this age (9 weeks old, or 6 weeks postinjection), the ONL was virtually depleted in the uninjected control eyes, but a significant number of photoreceptors had been preserved in the ONL of the eyes injected with iPS-RPE. The effects were quantified by counting the layers of nuclei in the ONL (right panel). (B): In vivo optical coherence tomography (OCT) images from 9-week-old control and injected RCS rat eyes across several weeks were taken and analyzed using a spectral-domain OCT system (Spectralis, Heidelberg Engineering). The red lines mark the inner layer of the retina (top) and the photoreceptor outer segment (POS)/RPE interface (bottom). The green reference line marks the point where the thickness measurements were calculated and plotted (right panel). (C): Regions of the eyes where 1F-iPS-RPE cells had successfully integrated were analyzed as described above. For this analysis, 25 images were taken across the region marked with a grid. Thickness measurements from this region are shown as a heat map (middle panel) and as averaged values (right panel). Note that the thickest regions correlate with the region in the fundus image where RPE cells were detected (the RPE cells in albino RCS rats do not synthesize melanin pigment). (D): Fundus image of an RCS rat with 1F-iPS-RPE cells implanted ( $n = 4$ ; representative image and traces are shown). The red circle (a) marks where the light beam was aimed in the eye over the 1F-iPS-RPE implanted region; the resulting electrical activity is shown in the trace labeled (a) in the middle panel and quantified in the right panel. The blue circle (b) marks where no cells were implanted; a significantly lower response was detected from this region (shown in the middle panel and quantified in the right panel). Focal electroretinography was used to test the electrical activity in RCS rat eyes injected with PBS. Activity in these eyes was similar to that of uninjected controls. Abbreviations: Ave., average; iPS, induced pluripotent stem; ONL, outer nuclear layer; PBS, phosphate-buffered saline; RPE, retinal pigment epithelium.



ERG have been largely unsuccessful since RPE incorporate into such a small region of the retina. Using fERG, we could focus on a discrete region of the retina (0.7%) and adjust the diameter and intensity of the light beam to deliver a stimulus directly onto the area of interest, and a corneal electrode on the front of the lens measured the elicited electrical response. Fundus images of the regions from which the recordings were measured could also be captured (Fig. 5D). When light was injected into regions into which 1F-iPS-RPE had incorporated, we detected significantly more electrical activity than when it was injected into regions in which no cells have been transplanted (Fig. 5D, middle and right panels), from eyes injected with only PBS (Fig. 5D), and from the contralateral uninjected eyes (data not shown). Collectively, therefore, we demonstrated significant anatomical and functional rescue of photoreceptors in RCS rat retinas in which 1F-RPE were implanted.

## DISCUSSION

The recent development of the iPSC reprogramming technology allows, for the first time, the generation of autologous cellular central nervous system grafts from readily accessible cell sources such as skin biopsies [1, 2]. AMD may represent an ideal target for autologous iPSC-RPE transplantation therapy, as RPE cell dysfunction in this disease is caused by cellular aging processes rather than a monogenic defect. Although several genetic risk alleles for AMD have been identified [53], manifestation age of AMD even in the presence of these risk alleles is above 55 years. Hence, iPSC-RPE cell grafts from AMD patients would be expected to represent younger, and presumably healthier, RPE that have not yet themselves become damaged by the aging processes. Furthermore, RPE cell grafts, unlike neuronal cell grafts, would not require synaptic integration into the retinal neuronal network to resume rescue activity and can be delivered locally into the subretinal space, thus avoiding the need for graft cell migration to their final localization.

Recent studies using transcriptomic analyses demonstrated significant differences between gene transcription in hES/hiPS-derived RPE and hRPE [27]. Although useful for monitoring the differentiation status of cells, variations in gene expression at the transcriptional level do not necessarily provide insight into cellular activities. Functional consequences of transcriptional activity can be analyzed with novel metabolomic-based analyses that quantitatively measure the activities of endogenous biochemical pathways [54–56]. We demonstrated in this study that the metabolomic profiles of 1F-iPS-RPE, 4F-iPS-RPE, and hRPE were remarkably similar, although 7.9% of detected features were dysregulated in 1F-iPS-RPE and 4F-iPS-RPE (but only 0.5% of the detected features were dysregulated in 1F-iPS-RPE versus hRPE). These findings suggest that the directed differentiation technique reported in this study yields high-quality RPE cells that have metabolomic profiles that strongly resemble those of young primary hRPE, making them very well suited for RPE replacement strategies. In fact, we show in this report using novel *in vivo* imaging techniques that 1F-iPS-RPE prevent retinal degeneration in a model of RPE-mediated retinal degeneration. The implantation of 1F-iPS-RPE in the subretinal space of RCS rats prevents thinning of the retina and photoreceptor cell death up to 24 weeks (6 months) after implantation without inducing tumorigenesis.

Further evidence suggesting that 1F-iPS-RPE represent a young, viable, albeit more differentiated source of autologous RPE was collected using proteomic approaches. The results of the targeted antibody-based proteomic *in-cell* Western assay revealed that 1F-iPS-RPE were more similar to hRPE than to hRPE from older donors or immortalized hRPE. The direct comparison of 1F-iPS-RPE with hRPE revealed that the most statistically significant differences were observed in advanced differentiation markers, including RPE65, bestrophin, and CRALBP. Furthermore, the levels of PEDF secreted by 1F-iPS-RPE were dramatically elevated, and pronounced melanin pigmentation was observed, further supporting our claim that 1F-iPS-RPE represent highly differentiated RPE cells. Cumulatively, these results suggest that the 1F-iPS-RPE-differentiation state strongly resembles that of young primary hRPE but is more mature than the hRPE we used in these experiments. 1F-iPS-RPE are also functional *in vivo*. Not only did they prevent accumulation of A2E and restore retinal recycling in RCS rat retinas, photoreceptors rescued by iPS-RPE transplantation elicited electrical responses when excited by light. These rescue effects were not elicited by sham injections. Notably, the implanted 1F-iPS-RPE cells continued to function by phagocytosing debris from the subretinal space well after the sensory retina had degraded.

One of the findings presented in this report could easily be interpreted in a different and less optimistic manner. The accumulation of lipofuscin- and drusen-like material in rodent eyes treated with iPSC-RPE resembles subretinal deposits observed in human patients with advanced AMD. We cannot exclude the possibility that the 1F-iPS-RPE may be aging prematurely (the average life span of a laboratory rat is thought to be between 2 and 3 years) or that they become unable to process ingested photoreceptor outer segments properly over time. However, the entire neural retina degenerates in RCS rats after 6 months, and this amount of degenerating tissue represents a massive phagocytic burden for 1F-iPS-RPE cells incorporated into only a discrete region of the eye (a much larger phagocytic load than would be encountered by these cells in a human patient). Published data from others suggest that during retinal degeneration, extreme retinal remodeling occurs, and photoreceptors, RPE cells, choriocapillaris, and Müller cells undergo severe metabolic stress [57]. Therefore, we suggest that such severe metabolic stress and overworking may be sufficient to induce the RPE phenotype observed 15 months after transplantation. We believe that the cumulative stress and phagocytosis of excessive numbers of shed outer segment membranes contribute to this phenotype; 7 months after transplantation, the 1F-iPS-RPE cells still appeared completely healthy. To substantiate this claim, 1F-iPS-RPE should be transplanted into a true mouse model of human geographic atrophy in which only a discrete region of the RPE and sensory retina is affected. Unfortunately, this type of model system is not currently available.

## CONCLUSION

Although this is not the first report of using iPSC-derived RPE cells to rescue retinal degeneration in dystrophic animals, this is the first study to use novel surgical, metabolomic, imaging, and electrophysiological techniques to characterize the rescued tissue and stem cell-derived cells, as well as to longitudinally track the rescue effect *in vivo*. Our data show that 1F-iPS-RPE strongly resemble hRPE that mediate strong anatomical and functional

rescue of photoreceptors in dystrophic animals, making them excellent replacements for diseased RPE in AMD patients. However, several issues still need to be addressed to advance this technology toward clinical application, including the further enhancement of differentiation time and efficiency and the development of adequate surgical techniques to successfully implant these cells into the subretinal space. Despite these yet unresolved tasks, transplantation of iPSC-RPE cells holds great promise for the treatment of blinding eye diseases.

#### ACKNOWLEDGMENTS

We acknowledge the expert assistance of Stephen Bravo (Friedlander Laboratory, Greg Sprehn (Phoenix Research Laboratories), and Dr. Malcolm R. Wood (Scripps Research Institute Core Microscopy Facility). We also thank Jennifer Trombley, RN, MSN, for excellent management of the human subjects and ESCRO components of this study and Michele Gerhart for outstanding administrative support. Part of the immunohistochemistry analysis was conducted using the Vanderbilt University Medical Center Cell Imaging Shared Resource, and we would like to thank Dr. Lillian B. Nanney for facilitating this. This work was supported by grants to M.F. from the California Institute of Regenerative Medicine (TR1-01219) and the National Eye Institute of the National

Institutes of Health (EY11254). T.U.K. is supported by a fellowship of the German Research Foundation (KR 2863/6-1). P.D.W. is supported by an F32 fellowship from the National Eye Institute (EY021416). T.K. is supported by the Manpei Suzuki Diabetes Foundation. D.F.F. is supported by the Vanderbilt University School of Medicine Emphasis Program. Present address of D.F.F.: Vanderbilt University School of Medicine, Nashville, Tennessee.

#### AUTHOR CONTRIBUTIONS

T.U.K. and P.D.W.: conception and design, collection and/or assembly of data, data analysis and interpretation, manuscript writing; T.K., D.F.F., A.S., and J.W.: conception and design, collection and/or assembly of data, data analysis and interpretation; M.L.: collection and/or assembly of data, data analysis and interpretation; A.L.D.: collection and/or assembly of data; W.L. and S.Z.: provision of study material; G.S.: data analysis and interpretation; S.D.: conception and design, data analysis and interpretation; M.F.: conception and design, data analysis and interpretation, manuscript writing, final approval of manuscript.

#### DISCLOSURE OF POTENTIAL CONFLICTS OF INTEREST

The authors indicate no potential conflicts of interest.

#### REFERENCES

- 1 Yu J, Vodyanik MA, Smuga-Otto K et al. Induced pluripotent stem cell lines derived from human somatic cells. *Science* 2007;318:1917–1920.
- 2 Takahashi K, Tanabe K, Ohnuki M et al. Induction of pluripotent stem cells from adult human fibroblasts by defined factors. *Cell* 2007;131:861–872.
- 3 Koch P, Kokaia Z, Lindvall O et al. Emerging concepts in neural stem cell research: Autologous repair and cell-based disease modelling. *Lancet Neurol* 2009;8:819–829.
- 4 Aoi T, Yae K, Nakagawa M et al. Generation of pluripotent stem cells from adult mouse liver and stomach cells. *Science* 2008;321:699–702.
- 5 Okita K, Ichisaka T, Yamanaka S. Generation of germline-competent induced pluripotent stem cells. *Nature* 2007;448:313–317.
- 6 Kim D, Kim CH, Moon JI et al. Generation of human induced pluripotent stem cells by direct delivery of reprogramming proteins. *Cell Stem Cell* 2009;4:472–476.
- 7 Markoulaki S, Hanna J, Beard C et al. Transgenic mice with defined combinations of drug-inducible reprogramming factors. *Nat Biotechnol* 2009;27:169–171.
- 8 Miura K, Okada Y, Aoi T et al. Variation in the safety of induced pluripotent stem cell lines. *Nat Biotechnol* 2009;27:743–745.
- 9 Bock C, Kiskinis E, Verstappen G et al. Reference Maps of human ES and iPSC cell variation enable high-throughput characterization of pluripotent cell lines. *Cell* 2011;144:439–452.
- 10 Hussein SM, Batada NN, Vuoristo S et al. Copy number variation and selection during reprogramming to pluripotency. *Nature* 2011;471:58–62.
- 11 Laurent LC, Ulitsky I, Slavin I et al. Dynamic changes in the copy number of pluripotency and cell proliferation genes in human ESCs and iPSCs during reprogramming and time in culture. *Cell Stem Cell* 2011;8:106–118.
- 12 Mayshar Y, Ben-David U, Lavon N et al. Identification and classification of chromosomal aberrations in human induced pluripotent stem cells. *Cell Stem Cell* 2010;7:521–531.
- 13 Li W, Zhou H, Abujarour R et al. Generation of human-induced pluripotent stem cells in the absence of exogenous Sox2. *STEM CELLS* 2009;27:2992–3000.
- 14 Zhu S, Li W, Zhou H et al. Reprogramming of human primary keratinocytes by Oct4 with chemical compounds. *Cell Stem Cell* 2010;7:651–655.
- 15 Strauss O. The retinal pigment epithelium in visual function. *Physiol Rev* 2005;85:845–881.
- 16 Congdon N, O'Colmain B, Klaver CC et al. Causes and prevalence of visual impairment among adults in the United States. *Arch Ophthalmol* 2004;122:477–485.
- 17 Resnikoff S, Pascolini D, Ety'ale D et al. Global data on visual impairment in the year 2002. *Bull World Health Organ* 2004;82:844–851.
- 18 Cahill MT, Freedman SF, Toth CA. Macular translocation with 360 degrees peripheral retinectomy for geographic atrophy. *Arch Ophthalmol* 2003;121:132–133.
- 19 Jousseaume AM, Joeres S, Fawzy N et al. Autologous translocation of the choroid and retinal pigment epithelium in patients with geographic atrophy. *Ophthalmology* 2007;114:551–560.
- 20 Idelson M, Alper R, Obolensky A et al. Directed differentiation of human embryonic stem cells into functional retinal pigment epithelium cells. *Cell Stem Cell* 2009;5:396–408.
- 21 Vugler A, Carr AJ, Lawrence J et al. Elucidating the phenomenon of HESC-derived RPE: Anatomy of cell genesis, expansion and retinal transplantation. *Exp Neurol* 2008;214:347–361.
- 22 Buchholz DE, Hikita ST, Rowland TJ et al. Derivation of functional retinal pigmented epithelium from induced pluripotent stem cells. *STEM CELLS* 2009;27:2427–2434.
- 23 Carr AJ, Vugler AA, Hikita ST et al. Protective effects of human iPSC-derived retinal pigment epithelium cell transplantation in the retinal dystrophic rat. *PLoS One* 2009;4:e8152.
- 24 Meyer JS, Shearer RL, Capowski EE et al. Modeling early retinal development with human embryonic and induced pluripotent stem cells. *Proc Natl Acad Sci U S A* 2009;106:16698–16703.
- 25 Osakada F, Jin ZB, Hiram Y et al. In vitro differentiation of retinal cells from human pluripotent stem cells by small-molecule induction. *J Cell Sci* 2009;122:3169–3179.
- 26 Hiram Y, Osakada F, Takahashi K et al. Generation of retinal cells from mouse and human induced pluripotent stem cells. *Neurosci Lett* 2009;458:126–131.
- 27 Liao JL, Yu J, Huang K et al. Molecular signature of primary retinal pigment epithelium and stem-cell-derived RPE cells. *Hum Mol Genet* 2010;19:4229–4238.
- 28 Soldner F, Hockemeyer D, Beard C et al. Parkinson's disease patient-derived induced pluripotent stem cells free of viral reprogramming factors. *Cell* 2009;136:964–977.
- 29 Cai J, Chen J, Liu Y et al. Assessing self-renewal and differentiation in human embryonic stem cell lines. *STEM CELLS* 2006;24:516–530.
- 30 Krohne TU, Holz FG, Kopitz J. Apical-to-basolateral transcytosis of photoreceptor outer segments induced by lipid peroxidation products in human retinal pigment epithelial cells. *Invest Ophthalmol Vis Sci* 2010;51:553–560.

- 31** Parish CA, Hashimoto M, Nakanishi K et al. Isolation and one-step preparation of A2E and iso-A2E, fluorophores from human retinal pigment epithelium. *Proc Natl Acad Sci U S A* 1998;95:14609–14613.
- 32** Wu YL, Yanase E, Feng XD et al. Structural characterization of bisretinoid A2E photocleavage products and implications for age-related macular degeneration. *Proc Natl Acad Sci U S A* 2010;107:7275–7280.
- 33** Smith CA, Want EJ, O'Maille G et al. XCMS: Processing mass spectrometry data for metabolite profiling using nonlinear peak alignment, matching, and identification. *Anal Chem* 2006;78:779–787.
- 34** O'Rahilly R. The prenatal development of the human eye. *Exp Eye Res* 1975;21:93–112.
- 35** Mircheff AK, Miller SS, Farber DB et al. Isolation and provisional identification of plasma membrane populations from cultured human retinal pigment epithelium. *Invest Ophthalmol Vis Sci* 1990;31:863–878.
- 36** Young RW, Bok D. Participation of the retinal pigment epithelium in the rod outer segment renewal process. *J Cell Biol* 1969;42:392–403.
- 37** Ohno-Matsui K, Morita I, Tombran-Tink J et al. Novel mechanism for age-related macular degeneration: An equilibrium shift between the angiogenesis factors VEGF and PEDF. *J Cell Physiol* 2001;189:323–333.
- 38** Sonoda S, Sreekumar PG, Kase S et al. Attainment of polarity promotes growth factor secretion by retinal pigment epithelial cells: Relevance to age-related macular degeneration. *Aging (Albany NY)* 2010;2:28–42.
- 39** Zhu D, Deng X, Spee C et al. Polarized secretion of PEDF from human embryonic stem cell-derived RPE promotes retinal progenitor cell survival. *Invest Ophthalmol Vis Sci* 2011;52:1573–1585.
- 40** Holz FG, Bellman C, Staudt S et al. Fundus autofluorescence and development of geographic atrophy in age-related macular degeneration. *Invest Ophthalmol Vis Sci* 2001;42:1051–1056.
- 41** von Rückmann A, Fitzke FW, Bird AC. In vivo fundus autofluorescence in macular dystrophies. *Arch Ophthalmol* 1997;115:609–615.
- 42** Sparrow JR, Yoon KD, Wu Y et al. Interpretations of fundus autofluorescence from studies of the bisretinoids of the retina. *Invest Ophthalmol Vis Sci* 2010;51:4351–4357.
- 43** Charbel Issa P, Bolz HJ, Ebermann I et al. Characterisation of severe rod-cone dystrophy in a consanguineous family with a splice site mutation in the MERTK gene. *Br J Ophthalmol* 2009;93:920–925.
- 44** Delori FC, Dorey CK, Staurenghi G et al. In vivo fluorescence of the ocular fundus exhibits retinal pigment epithelium lipofuscin characteristics. *Invest Ophthalmol Vis Sci* 1995;36:718–729.
- 45** Eldred GE, Lasky MR. Retinal age pigments generated by self-assembling lysosomotropic detergents. *Nature* 1993;361:724–726.
- 46** Liu J, Itagaki Y, Ben-Shabat S et al. The biosynthesis of A2E, a fluorophore of aging retina, involves the formation of the precursor, A2-PE, in the photoreceptor outer segment membrane. *J Biol Chem* 2000;275:29354–29360.
- 47** Gupta N, Brown KE, Milam AH. Activated microglia in human retinitis pigmentosa, late-onset retinal degeneration, and age-related macular degeneration. *Exp Eye Res* 2003;76:463–471.
- 48** Harada T, Harada C, Kohsaka S et al. Microglia-Müller glia cell interactions control neurotrophic factor production during light-induced retinal degeneration. *J Neurosci* 2002;22:9228–9236.
- 49** Lewis GP, Sethi CS, Carter KM et al. Microglial cell activation following retinal detachment: A comparison between species. *Mol Vis* 2005;11:491–500.
- 50** Katz ML, Redmond TM. Effect of Rpe65 knockout on accumulation of lipofuscin fluorophores in the retinal pigment epithelium. *Invest Ophthalmol Vis Sci* 2001;42:3023–3030.
- 51** Kim SR, Fishkin N, Kong J et al. Rpe65 Leu450Met variant is associated with reduced levels of the retinal pigment epithelium lipofuscin fluorophores A2E and iso-A2E. *Proc Natl Acad Sci U S A* 2004;101:11668–11672.
- 52** Thomas BB, Arai S, Ikai Y et al. Retinal transplants evaluated by optical coherence tomography in photoreceptor degenerate rats. *J Neurosci Methods* 2006;151:186–193.
- 53** Seddon JM, Reynolds R, Maller J et al. Prediction model for prevalence and incidence of advanced age-related macular degeneration based on genetic, demographic, and environmental variables. *Invest Ophthalmol Vis Sci* 2009;50:2044–2053.
- 54** Baker M. Metabolomics: From small molecules to big ideas. *Nat Methods* 2011;8:117–121.
- 55** Wikoff WR, Kalisak E, Trauger S et al. Response and recovery in the plasma metabolome tracks the acute LCMV-induced immune response. *J Proteome Res* 2009;8:3578–3587.
- 56** Yanes O, Clark J, Wong DM et al. Metabolic oxidation regulates embryonic stem cell differentiation. *Nat Chem Biol* 2010;6:411–417.
- 57** Marc RE, Jones BW, Watt CB et al. Extreme retinal remodeling triggered by light damage: Implications for age related macular degeneration. *Mol Vis* 2008;14:782–806.



**Generation of Retinal Pigment Epithelial Cells from Small Molecules and *OCT4* Reprogrammed Human Induced Pluripotent Stem Cells**

Tim U. Krohne, Peter D. Westenskow, Toshihide Kurihara, David F. Friedlander, Mandy Lehmann, Alison L. Dorsey, Wenlin Li, Saiyong Zhu, Andrew Schultz, Junhua Wang, Gary Siuzdak, Sheng Ding and Martin Friedlander

*Stem Cells Trans Med* 2012;1;96-109; originally published online February 6, 2012;

DOI: 10.5966/sctm.2011-0057

**This information is current as of February 28, 2012**

**Updated Information  
& Services**

including high-resolution figures, can be found at:  
<http://stemcellstm.alphaamedpress.org/content/1/2/96>

**Supplementary Material**

Supplementary material can be found at:  
<http://stemcellstm.alphaamedpress.org/content/suppl/2012/02/02/sctm.2011-0057.DC1.html>